Quantifying the seasonal variations and regional transport of $PM_{2.5}$ in the Yangtze River Delta region, China: Characteristics, sources, and health risks

Yangzhihao Zhan[a], Min Xie[a,g], Wei Zhao[b], Tijian Wang[a], Pulong Chen[c], Jun Tian[d], Kuanguang Zhu[e], Da Gao[f], Shu Li[a], Bingliang Zhuang[a], Mengmeng Li[a], Yi Luo[a], Runqi Zhao[a]

[a] School of Atmospheric Sciences, Nanjing University, Nanjing 210023, China
[b] Nanjing Institute of Environmental Sciences, Ministry of Ecology and Environment of the People's Republic of China, Nanjing 210023, China
[c] Net Zero Era (Jiangsu) Environmental Technology Co., Nanjing 210023, China
[d] Academy of Environmental Planning and Design. Co.,Ltd., Nanjing University, Nanjing 210023, China
[e] Hubei Provincial Academy of Eco-Environmental Sciences, Wuhan 430073, China
[f] State Key Joint Laboratory of Environment Simulation and Pollution Control, School of Environment, Tsinghua University, Beijing 100084, China
[g] School of Environment, Nanjing Normal University, Nanjing 210023, China

Correspondence to: Min Xie (minxie@nju.edu.cn), Wei Zhao (zhaowei@nies.org)

Abstract. Given the increasing complexity of the chemical composition of $PM_{2.5}$, identifying and quantitatively assessing the contributions of pollution sources has played an important role in formulating policies to control particle pollution. This study provides a comprehensive assessment between $PM_{2.5}$ chemical characteristics, sources, and health risks based on sampling data conducted over one year (March 2018 to February 2019) in Nanjing. Results show that $PM_{2.5}$ exhibits a distinct variation across different seasons, which is primarily driven by emissions, meteorological conditions, and chemical conversion of gaseous pollutants. First, the chemical mass reconstruction shows that secondary inorganic aerosols (SIA, 62.5 %) and carbonaceous aerosols (21.3%) contributed most to the $PM_{2.5}$ mass. The increasing oxidation rates of SO_2 and NO_2 from summer to winter indicate that the secondary transformation of gaseous pollutants is strongly positively correlated with relative humidity. Second, the positive matrix factorization (PMF) method shows that identified $PM_{2.5}$ sources include secondary inorganic aerosol sources (SIS, 42.5%), coal combustion (CC, 22.4%), industry source (IS, 17.3%), vehicle emission (VE, 10.7%), fugitive dust (FD, 5.8%) and other sources (1.3%). The Hybrid Single Particle Lagrangian Integrated Trajectory (HYSPLIT) model and the concentration-weighted trajectory (CWT) analysis are used to further explore different spatial distributions and regional transport of sources. The concentrations (10-11 $\mu g \cdot m^{-3}$) of SIS and CC distribute in Nanjing and central China in winter. The concentrations (8-10 $\mu g \cdot m^{-3}$) of IS and VE are potentially located north of Jiangsu, Anhui, and Jiangxi. Finally, the health risk assessment indicates that the carcinogenic and non-carcinogenic risks of toxic elements (Cr, As, Ni, Mn, V, and Pb) mainly come from IS, VE, and CC, which are within the tolerance or acceptable level. Although the main source of pollution in Nanjing is SIS at present, we should pay more attention to the health burden of vehicle emissions, coal combustion, and industrial processes.

1. Introduction

$PM_{2.5}$ is particulate matter with an aerodynamic equivalent diameter less than or equal to 2.5 μm, and one of the most important air pollutants, which can affect air quality (Sharma et al., 2020), atmospheric visibility (Tseng et al., 2019) and ecosystems (Li et al., 2021). $PM_{2.5}$ can directly enter the human body through the respiratory system and lead to increased health risks (Kumar et al., 2019; Sulaymon et al., 2021). $PM_{2.5}$ concentrations in the United States and Europe have begun to decrease since the 1980s, and those in Japan gradually decreased after 2012 (Zhang et al., 2020). In China, the annual average concentration of $PM_{2.5}$ has decreased by 50% with the implementation of the Air Pollution Prevention and Control Action Plan (APPCAP) in 2013. However, annual $PM_{2.5}$ concentrations in most cities are greater than 10 $\mu g \cdot m^{-3}$, the air quality guideline of the World Health Organization (Song et al., 2017; Zeng et al., 2019; Cheng et al., 2021), and the number of deaths caused by $PM_{2.5}$ exceeds one million per year (Zhu et al., 2020). It indicates that a comprehensive assessment between $PM_{2.5}$ chemical characteristics, sources, and health risks is significant for pollution control measures in the key regions of China.

Understanding the chemical composition of $PM_{2.5}$ is important for formulating control strategies. Sulfate, nitrate, and ammonium (SNA) are the major secondary inorganic aerosols, whose chemical conversion occurs in homogeneous and heterogeneous reactions (Fan et al., 2020; Chow et al., 2022). Variations in the form of SO_4^{2-} and NH_3 lead to variations in the acid-base balance of aerosols (Roper et al., 2019). Organic carbon (OC) comprises thousands of organic compounds. Elemental carbon (EC) is stable and mainly derived from primary sources of combustion products (Wu et al., 2020; Zhang et al., 2022). Both NO_3^-/SO_4^{2-} and OC/EC ratios can be reasonably used to evaluate the contribution of mobile and stationary sources to $PM_{2.5}$ in the atmosphere (Zhan et al., 2021). To identify the sources of $PM_{2.5}$, receptor modelings have been developed, which include positive matrix factorization (PMF), chemical mass balance (CMB), and principal component analysis (PCA) (Zong et al., 2016; Lv et al., 2020). Recently, the combination of the PMF model and trajectory modeling has proven to be powerful to identify source regions and quantify chemical compositions for a receptor site (Zheng et al., 2019). Air exposure models have been widely used to compare the health outcomes of people exposed to different levels of air pollution (Thurston et al., 2016; Conibear et al., 2018). Long-term exposure to $PM_{2.5}$ is particularly significant for cardiovascular disease mortality (Hayes et al., 2020). Trace metals (Cr, Ni, Mn, V, and Pb) are a minor component of $PM_{2.5}$ in qualitative terms, but the health risk of toxic elements through inhalation of $PM_{2.5}$ exceeds acceptable levels (Jiang et al., 2018; Jeong et al., 2019; Xie et al., 2020). Health risk assessments have been widely used to assess further the non-carcinogenic and carcinogenic health risks of toxic elements in $PM_{2.5}$ (Behrooz et al., 2021; Fang et al., 2021; Li et al., 2022).

Chemical characteristics of $PM_{2.5}$ have been widely investigated in the Beijing-Tianjin-Hebei (BTH), the Yangtze River Delta (YRD), and the Pearl River Delta (PRD) during the last decade (Huang et al., 2017; Liu et al., 2017; Li et al., 2020). In the megacity of China, the occurrence of haze may be exacerbated by interactions between aerosols and meteorological conditions and regional transport (Zeng et al., 2019; Fan et al., 2020; Wang et al., 2023). The YRD region is China's scientific research base and comprehensive transportation hub. The annual $PM_{2.5}$ concentration in the YRD has been reduced

by 45.6% from 2016 to 2018. However, as a mega-city in the YRD, the $PM_{2.5}$ in Nanjing still exceeds the National Ambient Air Quality Standard (35 $\mu g \cdot m^{-3}$ as an annual average) by more than 38 % (Nie et al., 2018). Source apportionment studies mainly focus on the relative importance of local emission and regional transportation on $PM_{2.5}$ at a specific site using the PMF model and the backward trajectory analysis (Zheng et al., 2019; Yan et al., 2021; Lv et al., 2022). Some studies involved the health risks of toxic elements in $PM_{2.5}$ (Zhang et al., 2019; Fang et al., 2021), and only a few studies discussed the classification of toxic elements according to PMF results (Wang et al., 2019; Wang et al., 2020). However, there were two shortcomings in previous studies: (1) Given the uneven geographical distribution of observation sites and difficulties in data collection, most studies were based on short-term data comparisons and lacked systematic comparisons of the distinctive seasonality, regional transport, and meteorological effects of various elements and sources. (2) A comprehensive assessment of the health risks of toxic elements in each source of $PM_{2.5}$ was still scarce, which limited the implementation of long-term pollution control measures in megacities.

In this work, we provide high-quality composition data for $PM_{2.5}$ in the typical YRD city, including their chemical characteristics and diurnal variations. Besides, the measured $PM_{2.5}$ in its entirety is successfully apportioned to various contributing sources by PMF and CWT methods. Finally, potential risks associated with exposure to airborne toxic elements are identified based on the health risk assessment. The results can systematically assess the relationship between chemical characteristics, sources, and health risks of $PM_{2.5}$, and serve to guide $PM_{2.5}$ control measures for other megacities.

2. Data and Methodology

2.1 Chemical component sampling, air quality and meteorological data

Hourly concentrations of particulate matter (PM) components from December 2018 to February 2019 in Nanjing were used in this study. The elemental carbon (EC), organic carbon (OC), 30 trace elements (Si, Al, As, Ca, K, Co, Mo, Ag, Sc, Tl, Pd, Br, Te, Ga, Cs, Pb, Se, Hg, Cr, Cd, Zn, Cu, Ni, Fe, Mn, Ti, Sb, Sn, and V), and 8 soluble components in aerosols (Na^+, K^+, Mg^{2+}, Ca^{2+}, Cl^-, NO_3^-, SO_4^{2-}, and NH_4^+) were quantified in each $PM_{2.5}$ sample. $PM_{2.5}$ samples were collected on the rooftop of the School of Atmospheric Sciences, Xianlin Campus, Nanjing University (32.12 °N, 118.96 °E). OC and EC were analyzed by the online carbon fraction Monitor (EA-32, Everisetech Co., Beijing). OC and EC were separated by step heating and then determined by the non-dispersive infrared method. The components of heavy metals were collected by the atmospheric heavy metal Monitor (AMS-100, Fpigroup Co., Hangzhou). The volumetric concentration of heavy elements ($ng \cdot m^{-3}$) was obtained by detecting the concentration of PM enriched on the filter membrane using the β ray absorption principle (Wang et al., 2020). The soluble components sampling instrument was the In-situ Gas and Aerosol Compositions Monitor (IGAC, Fortelice International Co., Taiwan). It consisted of the wet concentric circular tube, the gas gel processor, and the ion chromatograph. The sampling inlet was about 20 m above the ground and the flow rate was 16.67 $L \cdot min^{-1}$. The collected liquid samples were filtered by defoaming and then injected into the ion chromatography analyzers to analyze the

ion components from the gases and the aerosols. The detection limits were below 0.12 μg·m^{-3} and the collection efficiency was higher than 90% (Zhan et al., 2021).

Air pollutants, including $PM_{2.5}$, PM_{10}, O_3, NO_2, SO_2, and CO, were monitored by the National Environmental Monitoring Center (NEMC) of China. These data were issued hourly on the national urban air quality real-time publishing platform (https://air.cnemc.cn:18007/, last access: 7 April 2023). Meteorological parameters included air pressure, air temperature, relative humidity, wind speed, and boundary layer height. We collected hourly data from the National Climatic Data Center (NCDC) of the University of Wyoming website (http://weather.uwyo.edu/surface/, last access: 7 April 2023). Regarding boundary layer height, daily sounding vertical profiles were extracted from the national benchmark climate Nanjing station 58238 (32.00 °N, 118.48 °E) and were also acquired from this website. The quality assurance and quality control (QA/QC) procedures were used at each site according to the method of Xie et al. (2016) and Gao et al. (2021). $PM_{2.5}$ component data were collected hourly, and the study was based on high-time resolution data. We measured 10% of all samples as parallel sampling and the pass rate was over 95%. We defined the missing sampling of atmospheric pollutant data as -999 to facilitate PMF processing. The chemical mass reconstruction method was used to correct potential measurement errors, which was described in detail in Section 2.2. The QA/QC procedures have passed the artificial random inspection of extreme value and time consistency.

2.2 Mass and chemical composition determination for $PM_{2.5}$

Due to the limitation in sampling location and equipment, the sum of measured species was often lower than the gravimetric mass. Chemical mass reconstruction (CMR) attempted to achieve closure between the gravitational mass and the sum of components and correct potential measurement errors. In this study, the reconstructed result and the gravimetric result exhibited a significant correlation, with a mean R^2 of 0.93, indicating that the chemical reconstruction method had strong reliability. Following the work of Xu et al. (2021), eight categories of chemical components in chemically reconstructed $PM_{2.5}$ can be expressed as follows:

$$PM_{2.5} = OM + EC + MD + TM + SO_4^{2-} + NO_3^- + NH_4^+ + Cl^- \quad (1)$$

where OM refers to the organic matter. The OC to OM conversion coefficient at urban sites is 1.6 (Brokamp et al., 2017). The calculation of mineral dust (MD) is based on crustal element oxides (Yan et al., 2020):

$$MD = 2.14 \times Si + 1.67 \times Ti + 1.89 \times Al + 1.40 \times Ca + 1.58 \times Mn + 1.43 \times Fe + 1.21 \times K + 1.67 \times Mg \quad (2)$$

where Si is estimated as multiplying Al in crustal material by a converting factor (3.14) (Zheng et al., 2019). Trace metals (TM) represent the sum of 30 different types of heavy metals:

$$TM = As + Co + Mo + Ag + Sc + Tl + Pd + Br + Te + Ga + Cs + Pb + Se + Hg + Cr + Cd + Zn + Cu + Ni + Sb + Sn + V + Ba \quad (3)$$

2.3 Identification of source by the positive matrix factorization (PMF) model

The positive matrix factorization (PMF) was developed by the Environmental Protection Agency (EPA) and has been widely adopted to classify $PM_{2.5}$ into different factors (Zong et al., 2016). The US EPA PMF version 5.0 was referred to in

this study. The basic principle of the PMF model was to calculate the weight error of each chemical component in the particulate matter and then determined its main pollution source and contribution rate by the least square method (Paatero and Tapper, 1994). The equation of the PMF model can be expressed as follow:

$$X_{ij} = \sum_{k=1}^{p} g_{ik} f_{kj} + e_{ij} \quad (4)$$

where X_{ij} is the concentration of the *ij*th sample; g_{ik} represents the contribution of the *ik*th sample; f_{kj} represents the mass fraction of the *jk*th and e_{ij} is the residual between the measured mass concentration of the *ij*th sample and its analytical value. The purpose of the PMF model is to find the minimum Q value with the concentration file and uncertainty file (u_{ij}) introduced into the model. The objective function Q is defined as follows:

$$Q_{ij} = \sum_{i=1}^{n} \sum_{j=1}^{m} \left[\frac{X_{ij} - \sum_{k=1}^{p} g_{ik} f_{kj}}{u_{ij}} \right]^2 \quad (5)$$

where Q is the sum of all sample residuals and their uncertainties u. In this study, the fitting species included 41 types of chemical species of $PM_{2.5}$ that were selected and validated to ensure that the value of the objective function Q was minimized.

$$Unc = \frac{5}{6} \times MDL \quad (6)$$

$$Unc = \sqrt{(Error\ Fraction \times concentration)^2 + (0.5 \times MDL)^2} \quad (7)$$

where Unc is the uncertainty. MDL is the method detection limi. If the concentration is less than or equal to the MDL provided, Unc is calculated using a fixed fraction of the MDL (Taylor et al., 2020). If the concentration is greater than the MDL, the calculation is based on the concentration fraction and MDL.

First, we excluded more than 50% of the dataset for species below the method detection limit (MDL) and retained 23 species that were significantly correlated with $PM_{2.5}$. Second, we calculated the uncertainty (Unc) for each species based on the concentration fraction and MDL (Taylor et al., 2020). Third, different numbers of factors were tested with random seeds in 20 iterations of each run. When the number of factors was set to six, the fitting degree of the model calculation results was the highest, with a correlation coefficient of 0.93, and the species almost showed a normal curve. Finally, the bootstrap (BS) and displacement (DISP), and BS-DISP diagnostic analysis were also used to evaluate the rationality of the apportioned factor profiles and contributions. BS is used to detect and estimate the disproportionate effects of a small set of observations on the solution and also, to a lesser extent, the effects of rotational ambiguity. The value of the F-peak strength was ensured

to be 0.5 to eliminate the rotation ambiguity. The mapping for each factor in this study was more than 80% from the BS run, indicating the six-factor solution was appropriate.

2.4 Source apportionment by backward trajectory calculation and CWT analysis

The Hybrid Single Particle Lagrangian Integrated Trajectory (HYSPLIT) model was developed by the National Oceanic and Atmospheric Administration (NOAA) and the Bureau of Meteorology Australia to simulate and analyze the movement, deposition, and diffusion of airflow. The reanalysis data with a spatial resolution of one degree and a temporal resolution of 6 h (00:00, 06:00, 12:00, and 18:00 UTC) were obtained from the Global Data Assimilation System (GDAS) (https://rda.ucar.edu/datasets/, last access: 7 April 2023). To locate the potential source areas for the corresponding components, we used the HYSPLIT model to analyze the backward trajectory of airflow from March 2018 to February 2019. 48-hour backward trajectories terminated at a height of 100 m above ground level were calculated at the starting point (32.07 °N, 118.78 °E). Due to the high uncertainty of a single backward trajectory, we drew multiple trajectories and performed cluster analysis. The cluster analysis was a multivariate statistical technique using the Angle Distance algorithm, which could quantify the relationship among the pollution concentrations in each source area (Shu et al., 2017).

The concentration-weighted trajectory (CWT) analysis was further used to determine the relative contribution of different areas. The CWT analysis was conducted by the TrajStat software, which was a GIS (geographic information system) application that enabled the user to visualize and analyze the spatial and meteorological data with multiple data formats (Feng et al., 2021). In this study, the meteorological data used for the HYSPLIT model and the CWT method remained the same. The CWT method divided the research area into small equal grids, set a standard value for the research object, and defined the trajectory exceeding the standard value as the pollution trajectory. According to the criteria of the Chinese National Ambient Air Quality Standards (NAAQS), the standard value of the $PM_{2.5}$ concentrations was 75 $\mu g \cdot m^{-3}$ in this study. The spatial resolution was 0.5×0.5 (Liu et al., 2018). The CWT method reflected the pollution degree of different trajectories by calculating the weight concentration of the airflow trajectory in potential source areas:

$$C_{ij} = \frac{1}{\sum_{i=1}^{M} \tau_{ijl}} \sum_{l=1}^{M} C_l \tau_{ijl} \quad (8)$$

where C_{ij} is the average weight concentration of grid ij, C_l is the pollutant concentration based on trajectory l that passes through grid ij, and τ_{ij} is the residence time of trajectory l in grid ij. Similarly, to reduce the uncertainty caused by the smaller n_{ij}, the CWT value is multiplied by the weight function as well (Wong et al., 2022):

$$W_{ij} = \begin{cases} 1.00 & (80 < n_{ij}) \\ 0.72 & (20 < n_{ij} \le 80) \\ 0.42 & (10 < n_{ij} \le 20) \\ 0.05 & (n_{ij} \le 100) \end{cases} \quad (9)$$

where n_{ij} is the number of trajectories that pass through the ijth cell. W_{ij} is an empirical weight function to reduce the undue influence of small n_{ij} on the CWT values (Fan et al., 2019). In this study, the CWT value of each identified source derived from the PMF model was calculated.

2.5 Health risk assessment

The human health risk from heavy metals in $PM_{2.5}$ may occur through exposure to ambient air (Zhang et al., 2019). Based on the PMF analysis, we selected six toxic elements (Cr, As, Ni, Mn, V, and Pb) for the exposure risk assessment. Cr, Ni and As have both carcinogenic and non-carcinogenic effects, Mn and V mainly have non-carcinogenic effects, and Pb mainly produces a carcinogenic effect (Jiang et al., 2018). The non-carcinogenic and carcinogenic risks from the toxic species of $PM_{2.5}$ were evaluated by the hazard quotient (HQ) and lifetime carcinogenic risk (LCR), respectively. The US EPA human health risk assessment models were used to conduct carcinogenic and non-carcinogenic risk assessments (Khan et al., 2016):

$$EC_{inh} = \frac{GA \times ET \times EF \times ED}{AT} \quad (10)$$

$$HQ = \frac{EC_{inh}}{RfC_i \times 1000 \mu g \cdot mg^{-1}} \quad (11)$$

$$LCR = IUR \times EC_{inh} \quad (12)$$

where EC_{inh} is the average daily exposure concentration of toxic elements inhaled through respiration. GA is the concentration of toxic elements in each source composition. ET is the exposure time, 24 h·d^{-1}; EF is the exposure frequency, 365 d·yr^{-1}; ED is the exposure duration, 30 yr; and AT is the average exposure time, calculated by ED yr × 365 d·yr^{-1} × 24 h·d^{-1} for non-carcinogens and 70 yr × 365 d·yr^{-1} × 24 h·d^{-1} for carcinogens. RfC_i is the inhalation reference concentration (mg·m^{-3}). IUR is the inhalation unit risk((μg·m^{-3})$^{-1}$). HQ greater than 1 indicated a non-carcinogenic risk to human health. For carcinogenic risk, LCR < 10^{-6} means no cancer risk, LCR between 10^{-6} and 10^{-4} is acceptable or tolerable, and LCR > 10^{-4} is intolerable. The exposure parameters were shown in Table 1 (Jiang et al., 2018; Zhang et al., 2019).

Table 1. Exposure parameters of toxic elements through inhalation route in health risk assessments.

Toxic elements	RfC_i (μg·m^{-3})$^{-1}$	IUR (mg·m^{-3})

Cr	1.0×10^{-4}	1.2×10^{-2}
As	1.5×10^{-5}	4.3×10^{-3}
Ni	1.4×10^{-5}	2.4×10^{-4}
Mn	5.0×10^{-5}	——
V	1.0×10^{-4}	——
Pb	——	1.2×10^{-5}

206

207 **3. Results and discussions**

208 **3.1 Chemical components, meteorological parameters and diurnal variations**

209 Table 2 shows the seasonal average of chemical components and meteorological parameters from March 2018 to
210 February 2019. In this study, March to May 2018 is defined as spring, June to August 2018 is defined as summer, September
211 to November 2018 is defined as fall, and December 2018 to February 2019 is defined as winter. The daily average
212 concentration of $PM_{2.5}$ ranged from 6.7 to 234.0 $\mu g \cdot m^{-3}$, with an annual average of 68.7 $\mu g \cdot m^{-3}$. The order of average
213 concentrations of $PM_{2.5}$ in each season was winter (113.9 $\mu g \cdot m^{-3}$) > spring (99.1 $\mu g \cdot m^{-3}$) > autumn (38.9 $\mu g \cdot m^{-3}$) > summer
214 (23.7 $\mu g \cdot m^{-3}$). Seasonal variations of $PM_{2.5}$ were closely related to emission and meteorological conditions. In spring, the
215 wind speed (WS) was higher (3.5 $m \cdot s^{-1}$) than those in other seasons. Pearson correlation showed that $PM_{2.5}$ concentrations
216 were significantly ($p<0.01$) correlated to WS ($r=-0.36$) in spring. In summer, high boundary layer height (BLH) (520.4m)
217 significantly reduced $PM_{2.5}$ concentrations. In autumn and winter, $PM_{2.5}$ showed significant correlations between
218 temperature ($r=-0.53$), relative humidity ($r=0.62$) and BLH ($r=-0.43$). Biomass emissions in most cities and industrial
219 emissions in industrial cities contribute 7-27% to $PM_{2.5}$ mass in applicable cities (Tao et al., 2017). Coal consumption and
220 population density have a significantly positive effect on $PM_{2.5}$ concentration (Zhou et al., 2018; Chow et al., 2022). The
221 highest level of $PM_{2.5}$ in winter was due to coal consumption, lower temperatures (4.9°C), higher humidity (79.6%), and
222 lower BLH (419.7m) than in summer.

223 The seasonal variation of anthropogenic emissions also considerably affected $PM_{2.5}$ concentrations. The order of the
224 major components in $PM_{2.5}$ was NO_3^- (20-31%) > SO_4^{2-} (16-27%) > NH_4^+ (11-19%) > mineral dust (8-14%) > OM (6-
225 14%) > EC (2-4%) > trace metals (2-3%) > Cl^- (1-3%). Sulfate, nitrate, and ammonium (SNA) accounted for 60% of the
226 total $PM_{2.5}$ and were closely related to the secondary transformation of gaseous precursors. The concentration ratio of NO_3^-
227 to SO_4^{2-} (NO_3^-/SO_4^{2-}) was used to differentiate the relative importance of nitrogen (generally related to vehicle emissions)
228 and sulfur (normally related to stationary sources) in the atmosphere (Liu et al., 2019). Over the past few years, the mass
229 ratio of NO_3^-/SO_4^{2-} was 2.13 in Ningbo, 1.89 in Hangzhou, and 1.21 in Beijing (Huang et al., 2017; Li et al., 2018). In this
230 study, the average ratios of NO_3^-/SO_4^{2-} were 1.81 in spring, 1.20 in summer, 2.34 in autumn, and 1.59 in winter, respectively,
231 indicating the enhanced secondary transformation of gaseous pollutants (e.g. SO_2, NOx, VOCs) during heavily polluted
232 periods (Liu et al., 2016; Liu et al., 2018). The oxidation rates of SO_2 and NO_2 need to be further investigated.
233 Carbonaceous aerosols (OM and EC) accounted for 12% and 14% of $PM_{2.5}$ in spring and winter, respectively. The large

increase in the number of coal fires used for residential heating in winter may increase the abundance of carbon-containing emissions, including OC, EC, and VOC_S (Islam et al., 2020). Compared with 2015, the concentrations of OM and EC decreased from 22.9% to 12.8% (Chen et al., 2017). This may be related to policies to control coal combustion and motor vehicle emissions, considering similar meteorological conditions in the two periods (Tao et al., 2017; Jeong et al., 2019).

Table 2. Seasonal average concentration of components of $PM_{2.5}$, in $\mu g \cdot m^{-3}$ and % in brackets, and meteorological parameters. T, RH, WS, and BLH represent air temperature, relative humidity, wind speed and boundary layer height, respectively.

Components and meteorological parameters	Spring	Summer	Autumn	Winter
$PM_{2.5}$	99.1	23.7	38.9	113.9
SO_4^{2-}	20.5 (20.7)	5.2 (21.9)	7.3 (18.8)	31.5 (27.7)
NO_3^-	16.9 (17.1)	5.3 (22.4)	9.8 (25.2)	27.2 (23.9)
NH_4^+	15.1 (15.2)	3.2 (13.5)	7.1 (18.3)	11.5 (10.1)
OM	11.7 (11.8)	1.6 (6.8)	4.1 (10.5)	11.0 (9.7)
EC	2.3 (2.3)	0.8 (3.4)	1.6 (4.1)	3.6 (3.2)
Mineral dust	13.2 (13.3)	2.3 (9.7)	2.7 (6.9)	8.7 (7.6)
Trace metals	2.7 (2.7)	0.5 (2.1)	0.5 (1.3)	1.6 (1.4)
Cl^-	2.7 (2.7)	1.6 (6.8)	0.8 (2.1)	1.7 (1.5)
T (°C)	18.8	27.6	19.4	4.9
RH (%)	86.5	58.2	73.1	79.6
WS ($m \cdot s^{-1}$)	3.5	2.9	2.7	2.1
BLH (m)	469.7	520.4	443.6	419.7

Figure 1 shows the diurnal variation of chemical components in $PM_{2.5}$. The seasonal differences were mainly reflected in the variation in the timing of peak values. In spring (Fig. 1a), the highest and lowest $PM_{2.5}$ concentrations were 143.6 $\mu g \cdot m^{-3}$ at 7:00 and 94.8 $\mu g \cdot m^{-3}$ at 14:00, respectively. The concentration of SNA had obvious diurnal variations. From 6:00 to 18:00, the average concentration of NO_3^- increased from 17.6 to 21.8 $\mu g \cdot m^{-3}$, while the average concentration of SO_4^{2-} decreased from 23.2 to 15.9 $\mu g \cdot m^{-3}$. In summer (Fig. 1b), the highest and lowest $PM_{2.5}$ concentrations were 23.5 $\mu g \cdot m^{-3}$ at 9:00 and 14.2 $\mu g \cdot m^{-3}$ at 14:00, respectively. The maximum concentration difference of SNA between day and night was less than 10 $\mu g \cdot m^{-3}$, indicating the study area was in a relatively stable background field (Chen et al., 2018). In autumn (Fig. 1c), the highest and lowest $PM_{2.5}$ concentrations were 77.1 $\mu g \cdot m^{-3}$ at 8:00 and 47.8 $\mu g \cdot m^{-3}$ at 16:00, respectively. The concentration of SNA increased at night and decreased during the day. The maximum concentration difference was more than 20 $\mu g \cdot m^{-3}$. In winter (Fig. 1d), from 18:00 to 23:00, the concentration of SNA increased from 74.5 $\mu g \cdot m^{-3}$ to 108.7 $\mu g \cdot m^{-3}$, with increasing rates of 8.5 $\mu g \cdot m^{-3} \cdot h^{-1}$. The height of the atmospheric boundary layer decreased early in the winter

afternoons (Chen et al., 2018). The values of $PM_{2.5}$ in winter were higher at night due to the coal combustion and biomass burning (BB) for residential heating (Zou et al., 2017). In summary, compared with the spring and winter, $PM_{2.5}$ presented similar and relatively flat diurnal patterns in both autumn and summer. Although the seasonal variations of mass concentrations and aerosol compositions were substantially different, the concentrations of aerosol species showed similar diurnal variation patterns during all the sampling days with higher values in the nighttime and early morning, suggesting that the factors driving the diurnal variations were similar.

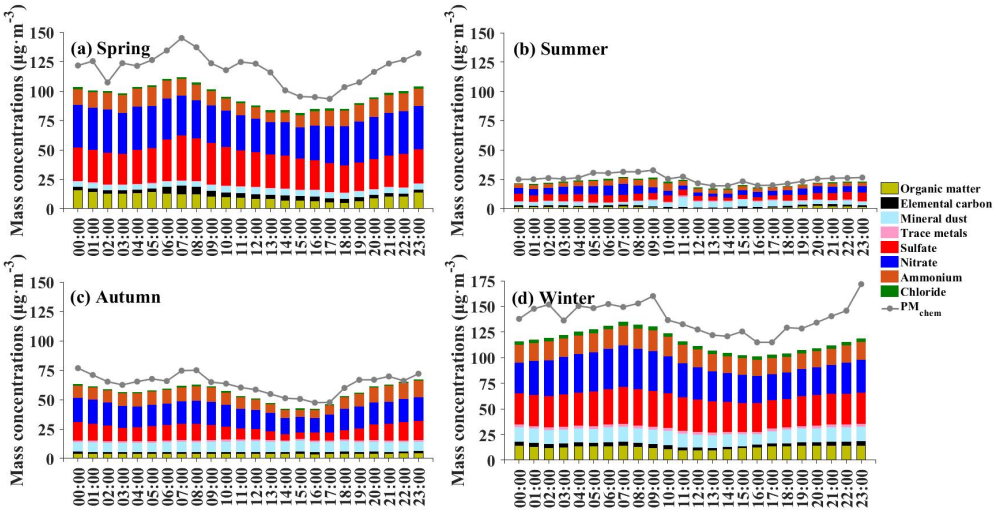

Figure 1. Average diurnal variation of the concentrations of major chemical components of $PM_{2.5}$ per each season.

3.2 Variation of $PM_{2.5}$ chemical compositions at different pollution levels

Figure 2 presents the $PM_{2.5}$ concentrations and components at different pollution levels. In this study, it was defined as the clean day (C) when the daily average $PM_{2.5}$ concentrations were less than 35 $\mu g \cdot m^{-3}$, the moderate pollution day (MP) when $PM_{2.5}$ concentrations were more than 35 $\mu g \cdot m^{-3}$ and less than 150 $\mu g \cdot m^{-3}$, and the heavy pollution day (HP) when $PM_{2.5}$ concentrations were more than or equal to 150 $\mu g \cdot m^{-3}$. As shown in Figure 2a, the annual average concentration of the water-soluble inorganic ions (WSIIs) was 41.9 $\mu g \cdot m^{-3}$, and accounted for 61.8% of $PM_{2.5}$. WSIIs were largely responsible for the variability in $PM_{2.5}$. The ratios of SNA in spring and winter were similar, with ratios of 65.0% for clean days, 75.0% for moderate pollution days, and 83.9% for heavy pollution days. With the degradation of air quality, the contribution of NO_3^- noticeably increased from 27.5% to 47.8% in spring and from 28.9% to 44.7% in autumn. To understand the oxidation rates of SO_2 and NO_2, the sulfur oxidation rate and nitrogen oxidation rate (defined as SOR = $SO_4^{2-}/(SO_4^{2-}+SO_2)$ and NOR = $NO_3^-/(NO_3^- + NO_2)$) were calculated. The critical value of SOR and NOR in the atmosphere are both 0.1 (Win et al., 2020). The order of the seasonal average NOR was winter (0.21) > spring (0.18) > autumn (0.17) > summer (0.15), while the order of the seasonal average SOR was winter (0.51) > spring (0.43) > autumn (0.42) > summer (0.36). $PM_{2.5}$ pollution in winter is

associated with high RH and rapid production of particulate sulfate from the oxidation of SO_2 emitted by coal combustion (Wang et al., 2020). From summer to winter, the NOR and SOR values increased by 40.0% and 41.6%, respectively. SOR and NOR showed a strong positive correlation with relative humidity, with a correlation coefficient of 0.53 and 0.61, respectively. The contribution of coal combustion varied between 30 and 57% of $PM_{2.5}$ in winter (Zhang et al., 2017). Under the conditions of high coal combustion emissions and high RH, the rapid oxidation of SO_2 occurred to produce sulfate. The sensitivity of $PM_{2.5}$ to surface temperature, wind speed, and boundary layer height is negative, while the sensitivity to relative humidity is positive (Chen et al., 2018; Sulaymon et al., 2021). In summer, the correlation coefficients of $PM_{2.5}$ with RH, T, WS, and BLH were 0.42, -0.47, -0.15, and -0.23, respectively. In winter, the correlation coefficients of $PM_{2.5}$ concentration with RH, T, WS, and BLH were 0.74, -0.57, -0.31, and -0.32, respectively. High RH (79.6%), low temperature (4.9°C), low WS (2.1m·s^{-1}), and low BLH (419.7m) provided favorable conditions for the accumulation of $PM_{2.5}$.

Coal combustion, biomass burning, and motor vehicle emissions all lead to a remarkable increase in carbonaceous aerosols (Chow et al., 2022). As shown in Figure 2b, carbonaceous species also had a significantly enhanced contribution in the colder season compared to the warmer season. The seasonal differences might be related to the effects of meteorological conditions and source emissions. Pearson correlation showed that the relationships between OM and EC and meteorological parameters (T, RH, WS, and BLH) were not significant (Table 2). To explore the possible pollution sources, it is feasible to study the mass ratio of OC/EC under different pollution levels. OC comprises thousands of organic compounds. EC is stable and mainly derived from primary sources of combustion products (Zhang et al., 2017; Wu et al., 2020). The OC/EC mass ratio of motor vehicle emissions (1.1) is lower than that of coal combustion (2.7) and biomass burning (9.0) (Xu et al., 2021). In this study, the OC/EC ratios continuously decreased as air pollution got worse, and the values ranged from 6.1 (C), 4.1 (MP) to 3.9 (HP) in spring, from 6.2 (C) to 4.8 (MP) in autumn and from 4.3 (C), 2.7 (MP) to 1.3 (HP) in winter. The annual average ratio of OC/EC decreased by 56.1% from clean days to heavy pollution days. If the OC/EC values were in the range of 2.5-5.0, vehicle exhaust emissions were considered as the main source of OC and EC in aerosols, whereas if the OC/EC values were in the range of 5.0-10.5, coal combustion was considered the main source of OC and EC in aerosols (Gao et al., 2018; Liu et al., 2018). Distinct differences in the evolution of the OC/EC ratio on polluted days imply that mobile sources are likely more important. Both the increase in motor vehicle emissions and the formation of meteorological conditions conducive to pollutant accumulation contribute to the decrease in the OC/EC ratio

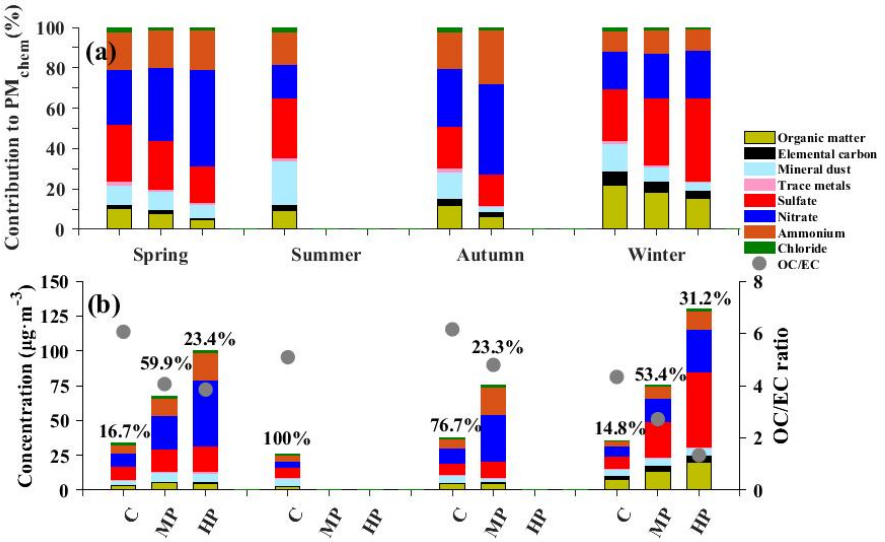

Figure 2. Chemical compositions of $PM_{2.5}$ and mass ratio of OC/EC at different pollution levels of the total samples per season. C, MP, and HP represent the clean day, moderately polluted day, and heavily polluted day, respectively. "%" represents the proportion of the filter sample quantity at each pollution level out of the total samples.

3.3 Source identification and apportionment

3.3.1 Elemental profile and source apportionment from the PMF model

To further quantitatively determine the source apportionment of $PM_{2.5}$, the EPA PMF5.0 model was adopted. The number of factors in the PMF model corresponded to the number of sources of $PM_{2.5}$ in this study. When the number of factors was set to six, the fitting degree of the model calculation results was the highest. Figure 3 presents the factor profiles and relative contributions of six factors to each species (% of species total), including secondary inorganic aerosol source (SIS), coal combustion (CC), industry source (IS), vehicle emission (VE), fugitive dust (FD), and other sources (OS). The meaning of % is the proportion of each chemical component in each source of $PM_{2.5}$. As shown in Figure 3a, the compositions of SIS were more clear than other sources. NO_3^- and SO_4^{2-} are mainly from the oxidation of NO_X and SO_2, while NH_4^+ probably comes from the conversion processes between ammonia and sulfuric and nitric acid (Win et al., 2020). Factor 1 was identified as the SIS with distinctly high loads of NH_4^+ (66.9%), NO_3^- (61.9%), SO_4^{2-} (63.8%) and Cl^- (55.3%). In Figure 3b, the high proportion of Pb (38.2%) and Se (45.1%) was identified in Factor 2, associating with moderate weighting on As (14.3%), SO_4^{2-} (20.5%), and Cl^- (22.2%). Pb and As are important identifying elements of coal combustion and are used as tracers (Xie et al., 2020). SO_4^{2-} is formed by the photochemical oxidation of sulfur-containing precursors (SO_2 and H_2S) released by coal combustion (Zong et al., 2016). Given the source profile, Factor 2 was related to coal combustion emissions. Factor 3 (Figure 3c) was characterized by the association of heavy metal pollutants such as As (42.8%), Pb (33.8%), Cr (61.1%), Zn (58.9%), Cu (59.4%), Fe (38.3%), and Mn (40.1%). As, Pb, Cr, Fe and Mn are related to metal smelting and processing (Fang et al., 2021). However, the percentage of OC was only 11.3%, while rates of Zn

(58.9%) and Cu (59.4%) were higher in Factor 3 (Fig. 3c). Cu, Zn, and OC are used as tracers of a mixed source of traffic and industrial, and OC is the major pollutant in the vehicle exhaust (Wang et al., 2020). Compared to motor vehicle emissions, Factor 3 should be significantly influenced by industrial activities. Cu and Zn were mainly from industrial process sources. As discussed above, Factor 3 was attributed to the IS. Factor 4 (Figure 3d) was characterized by the association of vehicle emissions, with the high proportions of Ni (54.7%), V (80.5%), OC (55.4%), EC (79.8%), and NO_3^- (20.3%). VOCs and NOx released from vehicles were the precursors of the secondary organic compounds and nitrate in $PM_{2.5}$ and were important catalysts for increased atmospheric oxidation (Guevara et al., 2021). OC and EC are mainly from the vehicle exhaust, and Ni and V are usually tracers of heavy oil combustion (Wu et al., 2020; Veld., 2021). Factor 4 contained a high proportion of OC, EC, and NO_3^-, which could be considered as vehicle emission, while factor 4 contained Ni and V, which were also influenced by shipping emissions (Gao et al., 2018; Veld., 2021). As shown in Figure 3e, Factor 5 had relatively high proportions of Fe (31.1%), Ti (78.2%), K^+ (55.8%), Ca^{2+} (60.5%), and Mg^{2+} (48.3%). Ti, Fe, and Mg are both common crustal elements that can represent the source of mineral dust. K^+ and Ca^{2+} are considered to be significant tracers of biomass burning, which have obvious seasonal variations (Tong et al., 2020; Silva et al., 2022). Factor 5 was classified as the fugitive dust and biomass burning, including road dust, industrial dust, and soil dust. Factor 6 (Fig. 3f) was unidentified and could be affected by coal combustion, industrial processes, and biomass burning. In the absence of a clear designation of the source, Factor 6 was attributed to an erroneous contribution from a different source.

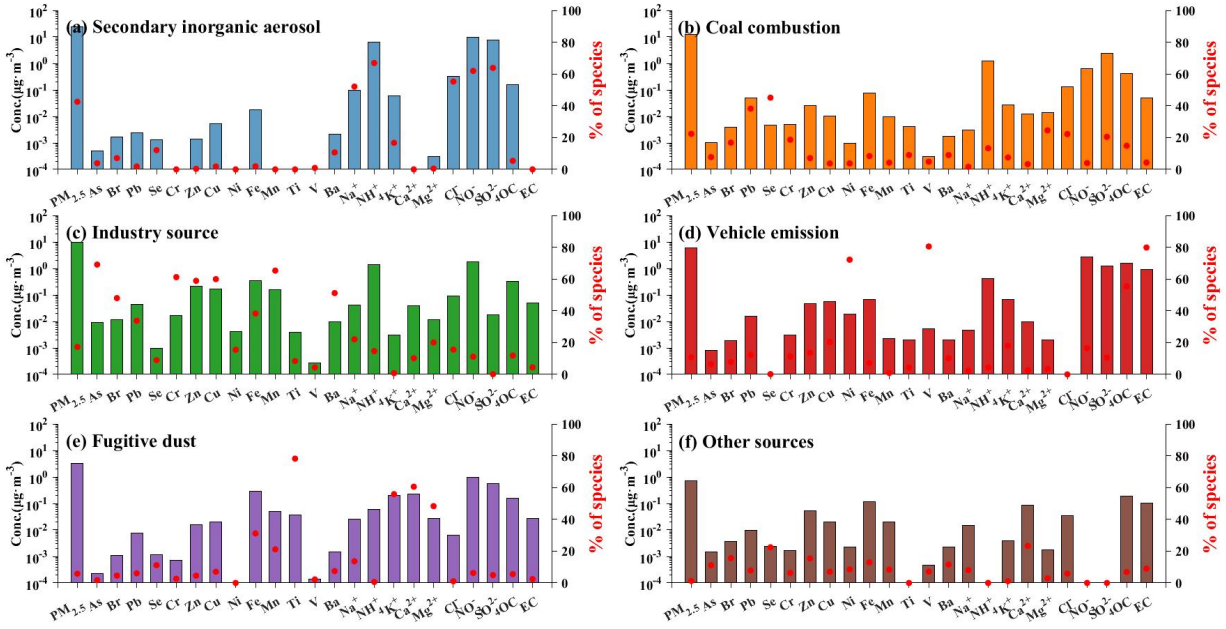

Figure 3. Factor profile in each source for $PM_{2.5}$ during the whole year. The histograms are the mass concentration of each species to every species ($\mu g \cdot m^{-3}$), and the red dots are the relative contributions of each source to every species (%).

Table 3 and Figure 4 show the comparisons of our PMF results with the previous findings. In the YED region, SIS contributed about 42.5% to $PM_{2.5}$ in Nanjing in this study, which was higher than that reported by Li et al. (2020), while the contributions of CC was lower. However, other sources of $PM_{2.5}$ in different cities were more complicated. In the BTH, IS was crucial source and contributed about 30% of Tianjin and Shijiazhuang (Huang et al., 2017). In contrast, IS in Nanjing contributed only 17.3% of $PM_{2.5}$ pollution. Recent emission control policies in the YRD have had positive effects on reducing industrial pollution. In the PRD, vehicle emissions, secondary nitrate, coal burning, and industrial emissions showed obvious local emission characteristics. An extra 30% $PM_{2.5}$ concentration was tightly related to local emissions in the downtown and industrial areas (Huang et al., 2014; Li et al., 2020; Chow et al., 2022). In this study, VE contributed only 10.7% in Nanjing. It is worth noting that the PMF model assumes that source profiles do not change significantly over time and that species do not undergo chemical reactions (Paatero and Tapper, 1994). The human activities under seasonal variations in this study made the actual pollution incompatible with the ideal assumption. For example, emissions from coal combustion increased the contribution of CC in winter significantly (Xu et al., 2021). In addition, the sources of air masses in each season also created uncertainties. All of these required detailed discussions of regional transport conditions in each season.

Table 3. Comparisons of source apportionment among different cities.

Location		Time	Main pollution sources (proportion)	Investigator
YRD	Nanjing	2018	SIS (42.5%); CC (22.4%); IS (17.3%); VE (10.7%); FD (5.8%)	This study
	Nanjing	2015	SIS (31.5%); CC (27.3%); Road dust (26.5%); Oil combustion (8.5%); IS (5.1%)	Li et al. (2020)
	Ningbo	2015	SIS (39.2%); VE (21.4%); CC (12.4%); IS (9.5%); Ship emission (7.4%); BB (5.1); Aged sea salt (3.7%)	Li et al. (2018)
BTH	Beijing	2017	SIS (35.6%); CC (30.8%); BB (17.6%); VE (12.4%); IS (6.3%)	Xu et al. (2021)
	Tianjin	2014	SIS (29.2%); IS (28.2%); CC (12.4%); VE (11.7%); Dust (11.7%); BB (5.3%)	Huang et al. (2017)
	Shijiazhuang	2014	SIS (36.4%); IS (27.3%); CC (15.5%); VE (8.5%); Dust (7.0%); BB (2.8%)	Huang et al. (2017)
PRD	Hong Kong	2015	SIS (44.9%); IS (13.5%); BB (10.8%); VE (8.6%); Oil combustion (5.3%); Aged sea salt (2.1%)	Chow et al. (2022)
	Shenzhen	2014	SIS (39.3%); VE (26.9%); BB (9.8%); Aged sea salt (4.7%); Dust (3.5)	Huang et al. (2014)
	Guangzhou	2014	SIS (34.6%); VE (28.6%); BB (23.1%); CC (17.7%); Ship emission (14.0%); IS (4.7%)	Li et al. (2020)

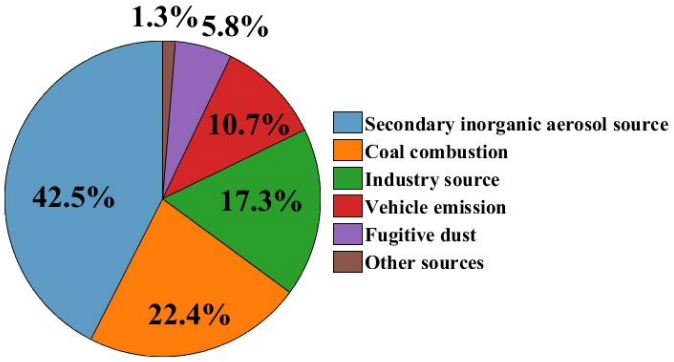

Figure 4. Average annual contribution of the sources identified for $PM_{2.5}$ in Nanjing in 2018.

3.3.2 Source identification by backward air mass trajectory analysis

The regional transport of air pollutants exerts a profound impact on local air quality (Shu et al., 2017). Figure 5 shows the quantified contributions of $PM_{2.5}$ with 48-h backward trajectories. In spring (Fig 5a), nearly half of the air masses (cluster a3) stemmed from northern Jiangxi, passed over Anhui Province before arriving at the sampling sites, and had the highest $PM_{2.5}$ average value (127.2 $\mu g \cdot m^{-3}$). CC from cluster a3 had the highest contribution with mass and percentage contributions being 41.0 $\mu g \cdot m^{-3}$ and 32.3%, respectively. In addition, FD contributed relatively highly in clusters a2 and a3, with proportions of 18.2% and 10.3%, respectively. Increased contribution from fugitive dust was related to industrial and construction activities (Xu et al., 2016). Cluster a2 originated in Liaoning and Cluster a3 was from northern Jiangxi. There were many industrial cities located in Liaoning, and the largest coal-fired thermal power plant in Jiangxi was located in the northern city of Jiujiang (Xu et al., 2016; Wang et al., 2019). Long-range transport of dust from these areas would have a high impact on the formation of severe particle pollution in the YRD. In summer (Fig 5b), the most obvious characteristic of regional transport was significantly influenced by the ocean. Clusters b2 and b3 were relatively clean with low concentrations of $PM_{2.5}$ (28.2 $\mu g \cdot m^{-3}$ for b2 and 32.4 $\mu g \cdot m^{-3}$ for b3). These clusters passed over the ocean areas and accounted for more than half of all trajectories. The magnitude of total CC, IS and VE exhibited a descending order from clusters b1 to b3. The dilution effects of clean ocean air masses played a vital role in particulate pollution. In autumn (Fig 5c), there were the highest concentrations of $PM_{2.5}$ in cluster c1, with an average value of 84.6 $\mu g \cdot m^{-3}$. CC (23.1%) and IS (27.6%) contributed relatively highly in cluster c1, indicating that regional transport from industrial regions might play an important role. For SIS, the proportion of NH_4^+ in these air masses was significantly higher in autumn than those in other seasons (Table 2). The increase in the proportion of NH_4^+ indicated that air pollution masses were heavily affected by nearby agricultural activities. In winter (Fig 5d), clusters d1 (108.3 $\mu g \cdot m^{-3}$) and d3 (122.6 $\mu g \cdot m^{-3}$) originated from Shandong Province and the BTH, accounting for more than three-quarters of the air masses. These air masses, which moved at high altitudes with a slow speed, could have carried abundant air pollutants. Cluster d2 (153.9 $\mu g \cdot m^{-3}$) was short-distance transport and derived from Jiangsu Province. The contribution of SIS exhibited a increasing order from clusters d1 (22.9%)

to d3 (43.4%) to d2 (55.5%), corresponding to the transition from long-range transport air masses to short-distance transport air masses.

Figure 6 shows the spatial distribution of the contribution from each source of $PM_{2.5}$ by the CWT method and highlighted the potential geographic origins. For SIS (Fig. 6a), the high levels (10-15 $\mu g \cdot m^{-3}$) of this source mainly originated from local emissions in Jiangsu and regional transport from Shandong Province. For CC (Fig. 6b), the high emissions (10-11 $\mu g \cdot m^{-3}$) were distributed in the YRD and central China. The weighted concentration values of CC were lower than those of the SIS. High concentrations near the center area are associated with local sources, while those far away from the center area are indicative of regional transport (Shu et al., 2017). The secondary aerosol source was probably from the accumulation of precursors emitted by local emissions. For IS and VE (Fig. 6c and d), there were no high potential areas for these sources. The moderate weighted concentration values of IS (8-10 $\mu g \cdot m^{-3}$) were potentially located in the north of Jiangsu, Anhui, and Jiangxi, which were the most important industrial base in China. The oceanic air masses are influenced by tropical cyclones with high temperature and strong wind (Li et al., 2018; Chow et al., 2022). Based on the backward trajectory calculation, most of the long-range transport of $PM_{2.5}$ passed through the Yellow Sea and the East Sea. High wind speed had a great effect on mitigating $PM_{2.5}$ pollution.

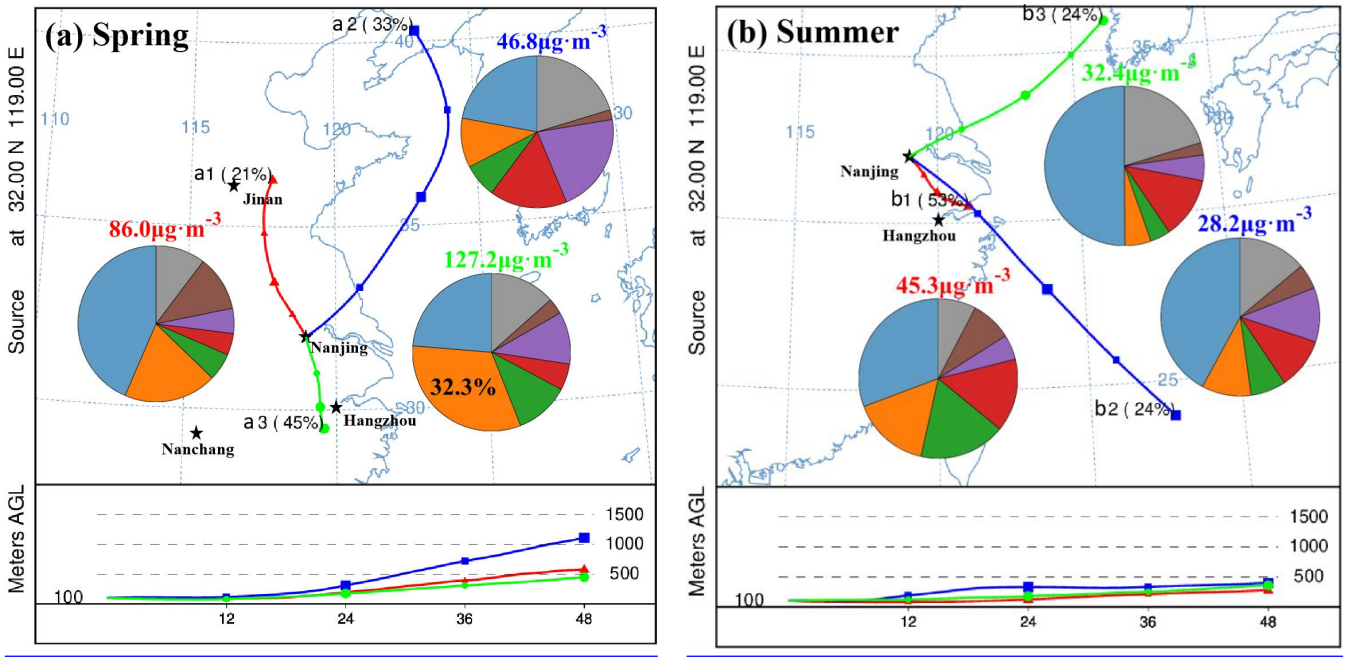

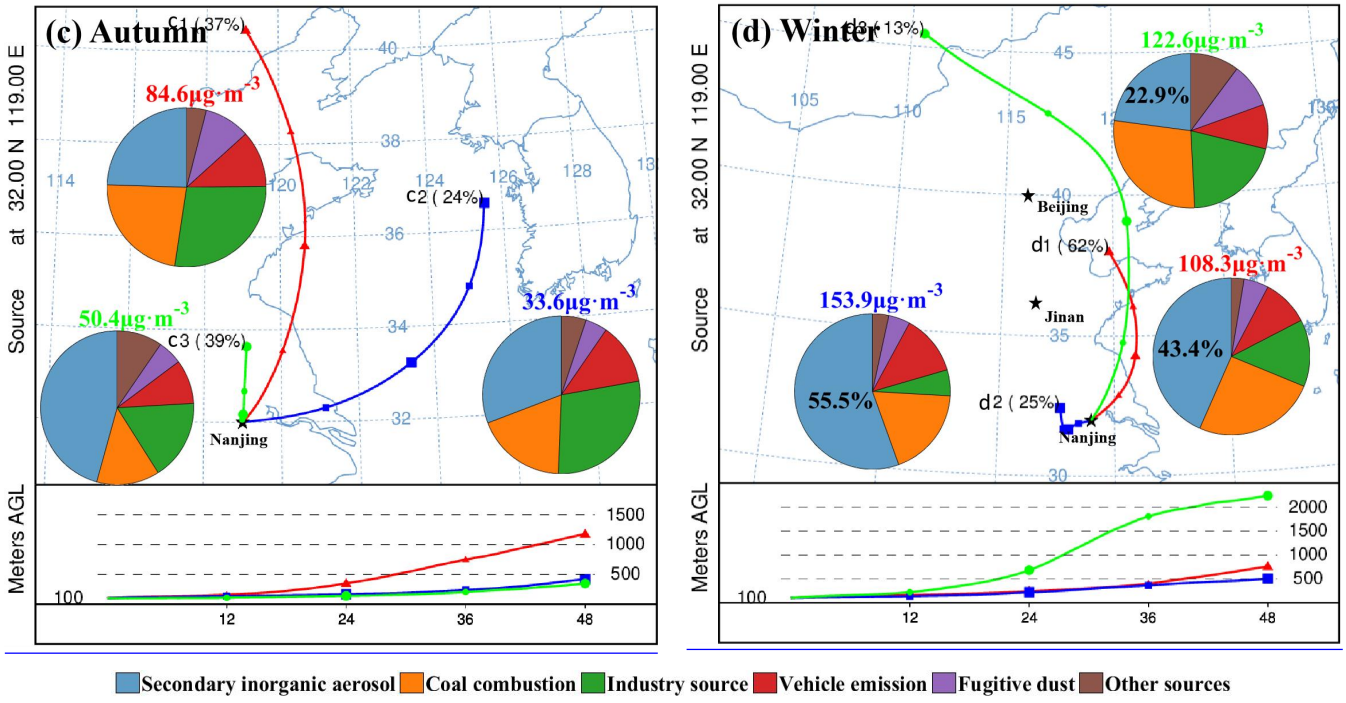

Figure 5. Source contributions to $PM_{2.5}$ grouped by air masses associated with different 48-h backward trajectory clusters. The pie charts show the average source contribution for corresponding clusters.

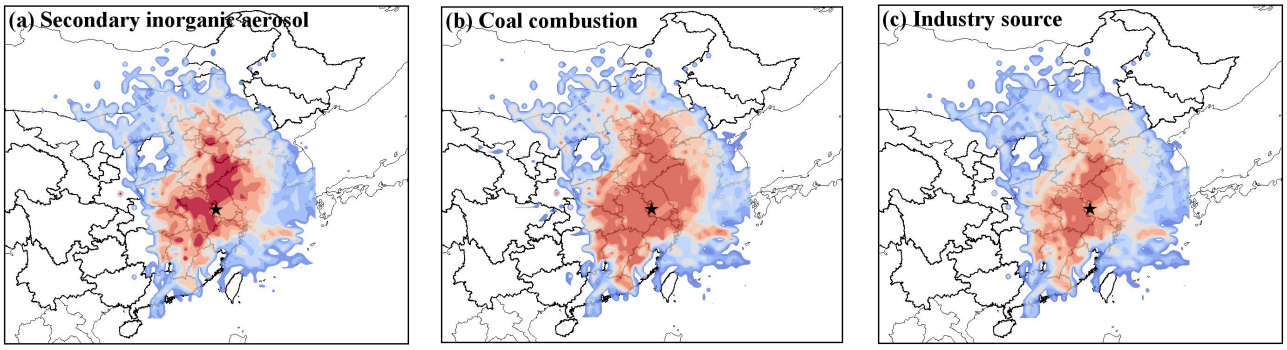

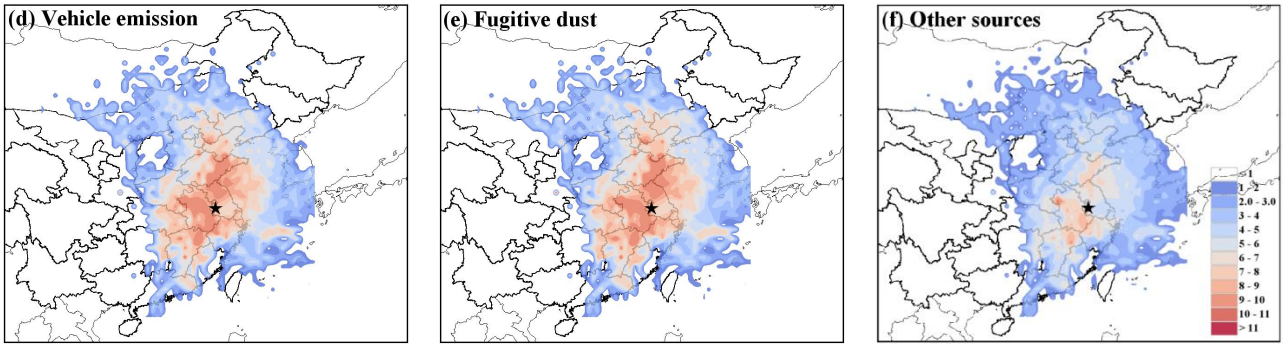

Figure 6. Potential source regions for individual sources of $PM_{2.5}$ identified by the CWT method from March 2018 to February 2019.

3.4 Non-carcinogenic and carcinogenic health risks of toxic metal elements in each source of $PM_{2.5}$

Figure 7 shows the HQ values of non-carcinogenic and the LCR values of carcinogenic risks in $PM_{2.5}$ and their total health risk in each source. For non-carcinogenic risk (Fig. 7a), the order of the average HQ values was Mn(0.47) > Ni (0.32) > As (0.14) > Cr (0.04) > V (0.02). The HQ values of toxic elements were all less than one, which indicated that there was no significant non-carcinogenic risk. However, the summation of five HQ values was higher than one, indicating that the combined exposure to the pollutant class still had adverse effects. The carcinogenic risk (Fig. 7b) posed by Ni (2.3×10^{-7}) and Pb (6.8×10^{-8}) were lower than 1×10^{-6} and could be acceptable. The carcinogenic risk level of Cr (1.0×10^{-7}) and As (1.8×10^{-5}) were within the tolerance or acceptable level (1×10^{-6}-1×10^{-4}) (Zheng et al., 2019). Figures 7 c and d show the integrated assessment of the source apportionment in toxic elements. IS accounted for the largest proportion of the non-carcinogenic and carcinogenic risk, with the HQ of 0.83 and the LCR of 5.8×10^{-6}, respectively. Although the PMF results indicated that SIS had the highest contribution to $PM_{2.5}$ (Fig. 4), the health risk results showed that the health risks of toxic elements from IS and CC were much higher than those from SIS. Previous studies showed that coal combustion sources in Beijing, Shanxi, and Jinan had higher respiratory exposure and health risks, while the fugitive dust source in Liaoning contained higher levels of Pb, As, and Co (Zeng et al., 2019). As, Cr, and Ni in $PM_{2.5}$ were within the acceptable level for both children and adults in Nanjing, but there was a potential carcinogenic risk posed by Pb via ingestion to children and adults (Hu et al., 2012). It was related to the differences in $PM_{2.5}$ pollution characteristics and source contributions in different cities. The ingestion exposure may result in the potential health risk from IS, CC, and VE. Based on the implementation of energy conservation and emission reduction policies, the main source of pollution in Nanjing is SIS at present, and the health risk has been alleviated. However, we should pay more attention to the health burden of vehicle emissions, coal combustion, and industrial processes.

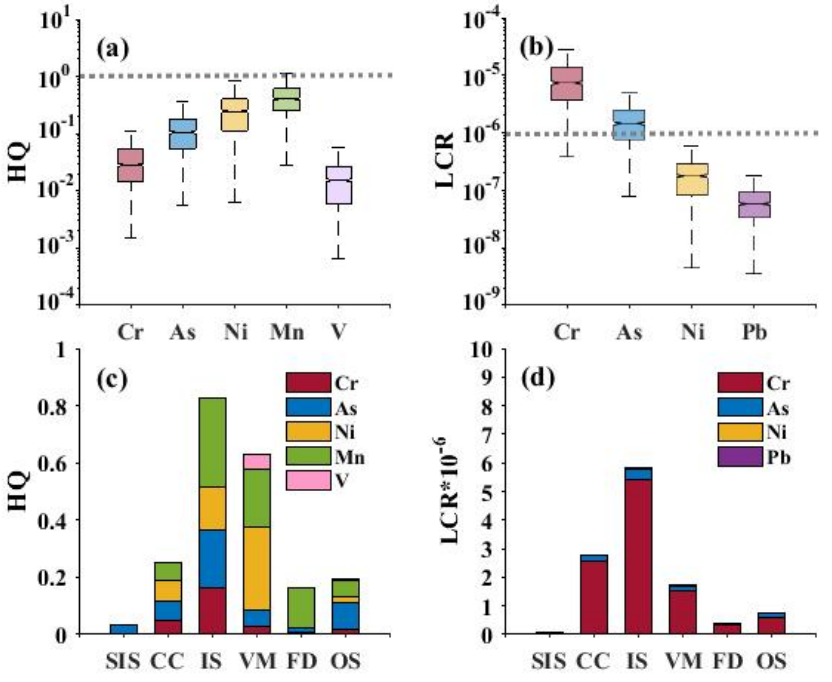

Figure 7. Non-carcinogenic (a) and carcinogenic (b) risks of toxic elements. Non-carcinogenic (c) and carcinogenic (d) risk of the sources identified for $PM_{2.5}$ in Nanjing.

3. Conclusions

Identifying and quantitatively assessing the contributions and health risks of pollution sources has played an important role in formulating policies to control particle pollution. We have derived a high-quality $PM_{2.5}$ composition data set, based on a chemical component monitoring from March 2018 to February 2019 in Nanjing. The PMF and back-trajectory results were adopted to investigate the chemical characteristics and regional transports of each source. The health risk assessment was used to explore non-carcinogenic and carcinogenic risks of toxic elements.

The results showed that $PM_{2.5}$ concentrations ranged from 6.7 to 234.0 $\mu g \cdot m^{-3}$, with an annual average of 68.7 $\mu g \cdot m^{-3}$. Water-soluble ions contributed the most to $PM_{2.5}$. From summer to winter, the NO_3^-/SO_4^{2-} ratio increased from 1.2 to 1.59. OC/EC ratio decreased by 56.1% from clean days to heavy pollution days. The average OC/EC ratio on heavy pollution days was 1.3. Both the increase in motor vehicle emissions and the formation of meteorological conditions conducive to pollutant accumulation contribute to the decrease in the OC/EC ratio. Based on the PMF model, the source variations and health risks were assessed. The contribution of identified sources (including SIS (42.5%), CC (22.4%), IS (17.3%), VE (10.7%), FD (5.8%), and other sources (1.3%)) had different spatial distributions and seasonal variations. The CWT analysis indicated that high emissions (10-11 $\mu g \cdot m^{-3}$) of SIS and CC were distributed in the YRD and central China in winter. Moderate emissions (8-9 $\mu g \cdot m^{-3}$) of IS and VE were potentially located in the north of Jiangsu, Anhui, and Jiangxi. The carcinogenic and non-carcinogenic risks of toxic elements (Cr, As, Ni, Mn, V, and Pb) mainly came from IS, VE, and CC, which were within the tolerance or acceptable level. Based on the implementation of energy conservation and emission reduction

policies, the main source of pollution in Nanjing is SIS at present, and the health risk has been alleviated. However, we should pay more attention to the health burden of vehicle emissions, coal combustion, and industrial processes.

This study provided new insight for $PM_{2.5}$ research between the source apportionment and health risk. The results presented characteristics of chemical components, pinpointed secondary transformation processes leading to the high $PM_{2.5}$ concentrations, revealed spatial variations of source contribution, and provided new references for mega-cities to conduct health risk analysis on air pollution control measures.

Data Availability.

$PM_{2.5}$ composition data were collected by the atmospheric heavy metal Monitor and the In-situ Gas and Aerosol Compositions Monitor in the School of Atmospheric Sciences, Nanjing University. Air quality monitoring data were acquired from the official NEMC real-time publishing platform (https://air.cnemc.cn:18007/, last access: 7 April 2023). Meteorological data were obtained from the University of Wyoming website (http://weather.uwyo.edu/, last access: 7 April 2023). The NCEP FNL data were taken from the NCEP (https://rda.ucar.edu/datasets/, last access: 7 April 2023). These data can be downloaded for free as long as one agrees to the official instructions.

Author contributions.

YZ and MX had original ideas, designed the research, collected the data, and prepared the original draft. YZ, WZ, YL, and RZ performed PMF experiments and carried out the data analysis. MX and WZ acquired financial support for the project leading to this publication. GD, TW, SL, BZ, and ML reviewed the initial draft and checked the English of the original paper.

Acknowledgments.

The authors are grateful to NEMC for the air quality monitoring data, to NCDC for the meteorological data, and to NCEP for global final analysis fields. We gratefully acknowledge the NOAA Air Resources Laboratory (ARL) for providing the HYSPLIT transport and dispersion model used in this work. We acknowledge the Chinese Academy of Meteorological Sciences for supporting this work (http://www.meteothink.org/, last access: 7 April 2023).

Competing interests.

The contact author has declared that neither they nor their co-author has any competing interests.

Financial support.

This research has been supported by the Natural Science Foundation of Jiangsu Province (grant no. BK20211158), the National Nature Science Foundation of China (grant no. 42275102), and the Basic Special Business Fund for R&D for the Central Level Scientific Research Institutes of Nanjing Institute of Environmental Sciences (grant no. GYZX210501)

References

Behrooz, R. D., Kaskaoutis, D. G., Grivas, G., and Mihalopoulos, N.: Human health risk assessment for toxic elements in the extreme ambient dust conditions observed in Sistan, Iran, Chemosphere, 262, https://doi.org/10.1016/j.chemosphere.2020.127835, 2021.

Brokamp, C., Jandarov, R., Rao, M. B., LeMasters, G., and Ryan, P.: Exposure assessment models for elemental components of particulate matter in an urban environment: A comparison of regression and random forest approaches, Atmos. Environ., 151, 1-11, https://doi.org/10.1016/j.atmosenv.2016.11.066, 2017.

Chen, D., Cui, H. F., Zhao, Y., Yin, L. N., Lu, Y., and Wang, Q. G.: A two-year study of carbonaceous aerosols in ambient $PM_{2.5}$ at a regional background site for western Yangtze River Delta, China, Atmos. Res., 183, 351-361, https://doi.org/10.1016/j.atmosres.2016.09.004, 2017.

Chen, Z. Y., Xie, X. M., Cai, J., Chen, D. L., Gao, B. B., He, B., Cheng, N. L., and Xu, B.: Understanding meteorological influences on PM2.5 concentrations across China: a temporal and spatial perspective, Atmos. Chem. Phys., 18, 5343-5358, https://doi.org/10.5194/acp-18-5343-2018, 2018.

Cheng, J., Tong, D., Zhang, Q., Liu, Y., Lei, Y., Yan, G., Yan, L., Yu, S., Cui, Y. R., Clarke, L., Geng, G. G., Zheng, B., Zhang, X. T., Davis, S. J., He, K. B.: Pathways of China's $PM_{2.5}$ air quality 2015–2060 in the context of carbon neutrality. National Science Review, 8(12), nwab078, https://doi.org/10.1093/nsr/nwab078, 2021.

Chow, W. S., Huang, X. H. H., Leung, K. F., Huang, L., Wu, X. R., and Yu, J. Z.: Molecular and elemental marker-based source apportionment of fine particulate matter at six sites in Hong Kong, China, Sci. Total Environ., 813, https://doi.org/10.1016/j.scitotenv.2021.152652, 2022.

Conibear, L., Butt, E. W., Knote, C., Arnold, S. R., and Spracklen, D. V.: Residential energy use emissions dominate health impacts from exposure to ambient particulate matter in India. Nature communications, 9(1), 617, https://doi.org/10.1038/s41467-018-02986-7, 2018.

Fan, H., Zhao, C. F., and Yang, Y. K.: A comprehensive analysis of the spatio-temporal variation of urban air pollution in China during 2014-2018, Atmos. Environ., 220, https://doi.org/10.1016/j.atmosenv.2019.117066, 2020.

Fang, B., Zeng, H., Zhang, L., Wang, H. W., Liu, J. J., Hao, K. L., Zheng, G. Y., Wang, M. M., Wang, Q., and Yang, W. Q.: Toxic metals in outdoor/indoor airborne $PM_{2.5}$ in port city of Northern, China: Characteristics, sources, and personal exposure risk assessment, Environ. Pollut., 279, https://doi.org/10.1016/j.envpol.2021.116937, 2021.

Feng, X. Y., Tian, Y. Z., Xue, Q. Q., Song, D. L., Huang, F. X., and Feng, Y. C.: Measurement report: Spatiotemporal and policy-related variations of PM2.5 composition and sources during 2015-2019 at multiple sites in a Chinese megacity, Atmos. Chem. Phys., 21, 16219-16235, https://doi.org/10.5194/acp-21-16219-2021, 2021.

Gao, D., Xie, M., Liu, J., Wang, T. J., Ma, C. Q., Bai, H. K., Chen, X., Li, M. M., Zhuang, B. L., and Li, S.: Ozone variability induced by synoptic weather patterns in warm seasons of 2014-2018 over the Yangtze River Delta region, China, Atmos. Chem. Phys., 21, 5847-5864, https://doi.org/10.5194/acp-21-5847-2021, 2021.

513 Gao, J. J., Wang, K., Wang, Y., Liu, S. H., Zhu, C. Y., Hao, J. M., Liu, H. J., Hua, S. B., Tian, H. Z.: Temporal-spatial
514 characteristics and source apportionment of $PM_{2.5}$ as well as its associated chemical species in the Beijing-Tianjin-Hebei
515 region of China, Environ. Pollut., 233, 714-724, https://doi.org/10.1016/j.envpol.2017.10.123, 2018.
516 Guevara, M., Jorba, O., Soret, A., Petetin, H., Bowdalo, D., Serradell, K., Tena, C., van der Gon, H. D., Kuenen, J., Peuch, V.
517 H., and Garcia-Pando, C. P.: Time-resolved emission reductions for atmospheric chemistry modelling in Europe during
518 the COVID-19 lockdowns, Atmos. Chem. Phys., 21, 773-797, https://doi.org/10.5194/acp-21-773-2021, 2021.
519 Hayes, R. B., Lim, C., Zhang, Y., Cromar, K., Shao, Y., Reynolds, H. R., Silverman, D. T., Jones, R. R., Park, Y., Jerrett, M.,
520 Ahn, J., and Thurston, G. D.: $PM_{2.5}$ air pollution and cause-specific cardiovascular disease mortality. International journal
521 of epidemiology, 49(1), 25-35, https://doi.org/10.1093/ije/dyz114, 2019.
522 Hu, X., Zhang, Y., Ding, Z. H., Wang, T. J., Lian, H. Z., Sun, Y. Y., and Wu, J. C.: Bioaccessibility and health risk of
523 arsenic and heavy metals (Cd, Co, Cr, Cu, Ni, Pb, Zn and Mn) in TSP and $PM_{2.5}$ in Nanjing, China, Atmos. Environ., 57,
524 146-152, https://doi.org/10.1016/j.atmosenv.2012.04.056, 2012.
525 Huang, X. F., Yun, H., Gong, Z. H., Li, X., He, L. Y., Zhang, Y. H., and Hu, M.: Source apportionment and secondary
526 organic aerosol estimation of $PM_{2.5}$ in an urban atmosphere in China. Sci. China Earth Sci. 57, 1352 – 1362 (2014).
527 https://doi.org/10.1007/s11430-013-4686-2, 2014.
528 Huang, X. J., Liu, Z. R., Liu, J. Y., Hu, B., Wen, T. X., Tang, G. Q., Zhang, J. K., Wu, F. K., Ji, D. S., Wang, L. L., and
529 Wang, Y. S.: Chemical characterization and source identification of $PM_{2.5}$ at multiple sites in the Beijing-Tianjin-Hebei
530 region, China, Atmos. Chem. Phys., 17, 12941-12962, https://doi.org/10.5194/acp-17-12941-2017, 2017.
531 Islam, M. R., Jayarathne, T., Simpson, I. J., Werden, B., Maben, J., Gilbert, A., Praveen, P. S., Adhikari, S., Panday, A. K.,
532 Rupakheti, M., Blake, D. R., Yokelson, R. J., DeCarlo, P. F., Keene, W. C., and Stone, E. A.: Ambient air quality in the
533 Kathmandu Valley, Nepal, during the pre-monsoon: concentrations and sources of particulate matter and trace gases,
534 Atmos. Chem. Phys., 20, 2927-2951, https://doi.org/10.5194/acp-20-2927-2020, 2020.
535 Jeong, C. H., Wang, J. M., Hilker, N., Debosz, J., Sofowote, U., Su, Y., Noble, M., Healy, R., Munoz, T., Celo, V., White, L.,
536 Audette, C., Herod, D., and Evans, G. J.: Temporal and spatial variability of traffic-related $PM_{2.5}$ sources: Comparison of
537 exhaust and non-exhaust emissions, Atmos. Environ., 198, 55-69. https://doi.org/10.1016/j.atmosenv.2018.10.038, 2019.
538 Jiang, N., Duan, S. G., Yu, X., Zhang, R. Q., and Wang, K.: Comparative major components and health risks of toxic
539 elements and polycyclic aromatic hydrocarbons of $PM_{2.5}$ in winter and summer in Zhengzhou: Based on three-year data,
540 Atmos. Res., 213, 173-184, https://doi.org/10.1016/j.atmosres.2018.06.008, 2018.
541 Khan, M. F., Latif, M. T., Saw, W. H., Amil, N., Nadzir, M. S. M., Sahani, M., Tahir, N. M., and Chung, J. X.: Fine
542 particulate matter in the tropical environment: monsoonal effects, source apportionment, and health risk assessment,
543 Atmos. Chem. Phys., 16, 597-617, https://doi.org/10.5194/acp-16-597-2016, 2016.
544 Kumari, P., and Toshniwal, D.: Impact of lockdown measures during COVID-19 on air quality- A case study of India, Int. J.
545 Environ. Health Res., 32, 503-510, https://doi.org/10.1080/09603123.2020.1778646, 2022.

546 Li, M., Hu, M., Guo, Q., Tan, T., Du, B., Huang, X., He, L., Guo, S., Wang, W., Fan, Y. and Xu, D.: Seasonal Source
547 Apportionment of $PM_{2.5}$ in Ningbo, a Coastal City in Southeast China, Aerosol Air Qual. Res, 18: 2741-2752.
548 https://doi.org/10.4209/aaqr.2018.01.0011, 2018.
549 Li, S. W., Chang, M. H., Li, H. M., Cui, X. Y., and Ma, L. Q.: Chemical compositions and source apportionment of $PM_{2.5}$
550 during clear and hazy days: Seasonal changes and impacts of Youth Olympic Games. Chem., 256, 127163,
551 https://doi.org/10.1016/j.chemosphere.2020.127163, 2020.
552 Li, T. T., Li, J., Jiang, H. X., Chen, D. H., Zong, Z., Tian, C. G., and Zhang, G.: Source Apportionment of PM(2.5)in
553 Guangzhou Based on an Approach of Combining Positive Matrix Factorization with the Bayesian Mixing Model and
554 Radiocarbon, Atmos, 11, https://doi.org/10.3390/atmos11050512, 2020.
555 Li, X. Y., Cheng, T. H., Shi, S. Y., Guo, H., Wu, Y., Lei, M., Zuo, X., Wang, W. N., and Han, Z. Y.: Evaluating the impacts
556 of burning biomass on regional transport under various emission conditions, Sci. Total Environ., 793,
557 https://doi.org/10.1016/j.scitotenv.2021.148481, 2021.
558 Li, X., Yan, C. Q., Wang, C. Y., Ma, J. J., Li, W. X., Liu, J. Y., and Liu, Y.: PM2.5-bound elements in Hebei Province,
559 China: Pollution levels, source apportionment and health risks, Sci. Total Environ., 806,
560 https://doi.org/10.1016/j.scitotenv.2021.150440, 2022.
561 Liu, J., Wu, D., Fan, S. J., Mao, X., and Chen, H. Z.: A one-year, on-line, multi-site observational study on water-soluble
562 inorganic ions in $PM_{2.5}$ over the Pearl River Delta region, China, Sci. Total Environ., 601, 1720-1732,
563 https://doi.org/10.1016/j.scitotenv.2017.06.039, 2017.
564 Liu, Y. K., Yu, Y. P., Liu, M., Lu, M., Ge, R. R., Li, S. W., Liu, X. R., Dong, W. B., and Qadeer, A.: Characterization and
565 source identification of PM2.5-bound polycyclic aromatic hydrocarbons (PAHs) in different seasons from Shanghai,
566 China, Sci. Total Environ., 644, 725-735, https://doi.org/10.1016/j.scitotenv.2018.07.049, 2018.
567 Liu, Z. R., Gao, W. K., Yu, Y. C., Hu, B., Xin, J. Y., Sun, Y., Wang, L. L., Wang, G. H., Bi, X. H., Zhang, G. H., Xu, H. H.,
568 Cong, Z. Y., He, J., Xu, J. S., and Wang, Y. S.: Characteristics of $PM_{2.5}$ mass concentrations and chemical species in
569 urban and background areas of China: Emerging results from the CARE-China network. Atmos. Chem. Phys., 18(12),
570 8849-8871, https://doi.org/10.5194/acp-18-8849-2018, 2018.
571 Liu, M. X., Huang, X., Song, Y., Tang, J., Cao, J. J., Zhang, X. Y., Zhang, Q., Wang, S. X., Xu, T. T., Kang, L., Cai, X. H.,
572 Zhang, H. S., Yang, F. M., Wang, H. B., Yu, J. Z., Lau, A. K. H., He, L. Y., Huang, X. F., Duan, L., Ding, A. J., Xue, L.
573 K., Gao, J., Liu, B., and Zhu, T.: Ammonia emission control in China would mitigate haze pollution and nitrogen
574 deposition, but worsen acid rain, Proc. Natl. Acad. Sci. U. S. A., 116, 7760-7765,
575 https://doi.org/10.1073/pnas.1814880116, 2019.
576 Liu, L., Zhang, J., Du, R. G., Teng, X. M., Hu, R., Yuan, Q., Tang, S. S., Ren, C. H., Huang, X., Xu, L., Zhang, Y. X.,
577 Zhang, X. Y., Song, C. B., Liu, B., Lu, G. D., Shi, Z. B., and Li, W. J.: Chemistry of atmospheric fine particles during the
578 COVID - 19 pandemic in a megacity of Eastern China. Geophys. Res.-Atmos.,, 48(2), 2020GL091611,
579 https://doi.org/10.1029/2020GL091611, 2020

Lv, Z. F., Wang, X. T., Deng, F. Y., Ying, Q., Archibald, A. T., Jones, R. L., Ding, Y., Cheng, Y., Fu, M. L., Liu, Y., Man, H. Y., Xue, Z. G., He, K. B., Hao, J. M., and Liu, H. A.: Source-Receptor Relationship Revealed by the Halted Traffic and Aggravated Haze in Beijing during the COVID-19 Lockdown, Environ. Sci. Technol., 54, 15660-15670, https://doi.org/10.1021/acs.est.0c04941, 2020.

Lv, L. L., Wei, P., Hu, J. N., Chen, Y. J., and Shi, Y. P.: Source apportionment and regional transport of PM2.5 during haze episodes in Beijing combined with multiple models, Atmos. Res., 266, https://doi.org/10.1016/j.atmosres.2021.105957, 2022.

Nie, D. Y., Chen, M. D., Wu, Y., Ge, X. L., Hu, J. L., Zhang, K., and Ge, P. X.: Characterization of Fine Particulate Matter and Associated Health Burden in Nanjing, Int. J. Env. Res. Public Health, 15, https://doi.org/10.3390/ijerph15040602, 2018.

Paatero, P., and Tapper, U.: POSITIVE MATRIX FACTORIZATION - A NONNEGATIVE FACTOR MODEL WITH OPTIMAL UTILIZATION OF ERROR-ESTIMATES OF DATA VALUES, Environmetrics, 5, 111-126, https://doi.org/10.1002/env.3170050203, 1994.

Sharma, S., Zhang, M. Y., Anshika, Gao, J. S., Zhang, H. L., and Kota, S. H.: Effect of restricted emissions during COVID-19 on air quality in India, Sci. Total Environ., 728, https://doi.org/10.1016/j.scitotenv.2020.138878, 2020.

Shu, L., Xie, M., Gao, D., Wang, T. J., Fang, D. X., Liu, Q., Huang, A. N., and Peng, L. W.: Regional severe particle pollution and its association with synoptic weather patterns in the Yangtze River Delta region, China, Atmos. Chem. Phys., 17, 12871-12891, https://doi.org/10.5194/acp-17-12871-2017, 2017.

Silva, L. F., Schneider, I. L., Artaxo, P., Núñez-Blanco, Y., Pinto, D., Flores, É. M., Gómez-Plata, L., Ramírez, O., and Dotto, G. L.: Particulate matter geochemistry of a highly industrialized region in the Caribbean: Basis for future toxicological studies, Geos. Front, 13(1), 101-115, https://doi.org/10.1016/j.gsf.2020.11.012, 2022.

Song, C. B., He, J. J., Wu, L., Jin, T. S., Chen, X., Li, R. P., Ren, P. P., Zhang, L., and Mao, H. J.: Health burden attributable to ambient $PM_{2.5}$ in China. Environ., Pollut., 223, 575-586, https://doi.org/10.1016/j.envpol.2017.01.060, 2017.

Sulaymon, I. D., Zhang, Y. X., Hopke, P. K., Zhang, Y., Hua, J. X., and Mei, X. D.: COVID-19 pandemic in Wuhan: Ambient air quality and the relationships between criteria air pollutants and meteorological variables before, during, and after lockdown, Atmos. Res., 250, https://doi.org/10.1016/j.atmosres.2020.105362, 2021.

Tao, J., Zhang, L., Cao, J., and Zhang, R.: A review of current knowledge concerning $PM_{2.5}$ chemical composition, aerosol optical properties and their relationships across China, Atmos. Chem. Phys., 17, 9485–9518, https://doi.org/10.5194/acp-17-9485-2017, 2017.

Taylor, A. A., Tsuji, J. S., Garry, M. R., McArdle, M. E., Goodfellow, W. L., Adams, W. J., and Menzie, C. A.: Critical Review of Exposure and Effects: Implications for Setting Regulatory Health Criteria for Ingested Copper, Environ. Manage., 65, 131-159, https://doi.org/10.1007/s00267-019-01234-y, 2020.

Thurston, G. D., Burnett, R. T., Turner, M. C., Shi, Y., Krewski, D., Lall, R., Ito, K., Jerrett, M., Gapstur, S. M., Diver, W. R., and Pope III, C. A.: Ischemic heart disease mortality and long-term exposure to source-related components of US fine particle air pollution. Environ. Health Pers., 124(6), 785-794, https://doi.org/10.1289/ehp.1509777, 2016.

Tong, S. Y., Kong, L. D., Yang, K. J., Shen, J. D., Chen, L., Jin, S. Y., Wang, C., Sha, F., and Wang, L.: Characteristics of air pollution episodes influenced by biomass burning pollution in Shanghai, China, Atmos. Environ., 238, https://doi.org/10.1016/j.atmosenv.2020.117756, 2020.

Tseng, C. H., Tsuang, B. J., Chiang, C. J., Ku, K. C., Tseng, J. S., Yang, T. Y., Hsu, K. H., Chen, K. C., Yu, S. L., Lee, W. C., Liu, T. W., Chan, C. C., and Chang, G. C.: The Relationship Between Air Pollution and Lung Cancer in Nonsmokers in Taiwan, J. Thorac. Oncol., 14, 784-792, https://doi.org/10.1016/j.jtho.2018.12.033, 2019.

Veld, M., Alastuey, A., Pandolfi, M., Amato, F., Perez, N., Reche, C., and Querol, X.: Compositional changes of PM2.5 in NE Spain during 2009–2018: A trend analysis of the chemical composition and source apportionment, Sci. Total Environ., 795, 148728, https://doi.org/10.1016/j.scitotenv.2021.148728, 2021.

Wang, S. S., Hu, G. R., Yan, Y., Wang, S., Yu, R. L., and Cui, J. Y.: Source apportionment of metal elements in $PM_{2.5}$ in a coastal city in Southeast China: Combined Pb-Sr-Nd isotopes with PMF method, Atmos. Environ., 198, 302-312, https://doi.org/10.1016/j.atmosenv.2018.10.056, 2019.

Wang, S. B., Ji, Y. Q., Zhao, J. B., Lin, Y., and Lin, Z.: Source apportionment and toxicity assessment of $PM_{2.5}$-bound PAHs in a typical iron-steel industry city in northeast China by PMF-ILCR, Sci. Total Environ., 713, https://doi.org/10.1016/j.scitotenv.2019.136428, 2020.

Wang, J. F., Li, J. Y., Ye, J. H., et al.: Fast sulfate formation from oxidation of SO_2 by NO_2 and HONO observed in Beijing haze. Nat. Commun., 11(1), 2844, https://doi.org/10.1038/s41467-020-16683-x, 2020.

Wang, H. L., Ke, Y., Tan, T., Zhu, B., Zhao, L. T., Yin, Y.: Observational evidence for the dual roles of BC in the megacity of eastern China: Enhanced O_3 and decreased $PM_{2.5}$ pollution, Chemosphere, 327, https://doi.org/10.1016/j.chemosphere.2023.138548, 2023.

Win, M. S., Zeng, J. Y., Yao, C. H., Zhao, M. F., Xiu, G. L., Xie, T. T., Rao, L. F., Zhang, L. Y., Lu, H., Liu, X. C., Wang, Q. Y., and Lu, S. N.: Sources of HULIS-C and its relationships with trace metals, ionic species in $PM_{2.5}$ in suburban Shanghai during haze and non-haze days, JAtC, 77, 63-81, https://doi.org/10.1007/s10874-020-09404-7, 2020.

Wong, Y. K., Liu, K. M., Yeung, C., Leung, K. K. M., and Yu, J. Z.: Measurement report: Characterization and source apportionment of coarse particulate matter in Hong Kong: insights into the constituents of unidentified mass and source origins in a coastal city in southern China, Atmos. Chem. Phys., 22, 5017-5031, https://doi.org/10.5194/acp-22-5017-2022, 2022.

Wu, X., Cao, F., Haque, M., Fan, M. Y., Zhang, S. C., and Zhang, Y. L.: Molecular composition and source apportionment of fine organic aerosols in Northeast China, Atmos. Environ., 239, https://doi.org/10.1016/j.atmosenv.2020.117722, 2020.

Xie, M., Liao, J. B., Wang, T. J., Zhu, K. G., Zhuang, B. L., Han, Y., Li, M. M., and Li, S.: Modeling of the anthropogenic heat flux and its effect on regional meteorology and air quality over the Yangtze River Delta region, China, Atmos. Chem. Phys., 16, 6071-6089, https://doi.org/10.5194/acp-16-6071-2016, 2016.

Xie, J. J., Yuan, C. G., Xie, J., Niu, X. D., and He, A. E.: PM2.5-bound potentially toxic elements (PTEs) fractions, bioavailability and health risks before and after coal limiting, Ecotoxicol. Environ. Saf., 192, https://doi.org/10.1016/j.ecoenv.2020.110249, 2020.

Xu, H. M., Cao, J. J., Chow, J. C., Huang, R. J., Shen, Z., Chen, L. A., Ho, K. F. and Watson, J. G.: Inter-annual variability of wintertime $PM_{2.5}$ chemical composition in Xi'an, China: evidences of changing source emissions, Sci. Total Environ., 545, 546-555, https://doi.org/10.1016/j.scitotenv.2015.12.070, 2016.

Xu, J. S., Liu, D., Wu, X. F., Vu, T., Zhang, Y. L., Fu, P. Q., Sun, Y. L., Xu, W. Q., Zheng, B., Harrison, R. M., and Shi, Z. B.: Source apportionment of fine organic carbon at an urban site of Beijing using a chemical mass balance model, Atmos. Chem. Phys., 21, 7321-7341, https://doi.org/10.5194/acp-21-7321-2021, 2021.

Yan, Y., Zheng, Q., Yu, R. L., Hu, G. R., Huang, H. B., Lin, C. Q., Cui, J. Y., and Yan, Y.: Characteristics and provenance implications of rare earth elements and Sr-Nd isotopes in $PM_{2.5}$ aerosols and $PM_{2.5}$ fugitive dusts from an inland city of southeastern China, Atmos. Environ., 220, https://doi.org/10.1016/j.atmosenv.2019.117069, 2020.

Yan, Y. C., Liu, Z. R., Gao, W., Li, J. Y., Zhang, X. H., Chai, W. H., Bai, J. H., Hu, B., and Wang, Y. S.: Physiochemistry characteristics and sources of submicron aerosols at the background area of North China Plain: Implication of air pollution control in heating season, Atmos. Res., 249, https://doi.org/10.1016/j.atmosres.2020.105291, 2021.

Zeng, Y. Y., Cao, Y. F., Qiao, X., Seyler, B. C., and Tang, Y.: Air pollution reduction in China: Recent success but great challenge for the future, Sci. Total Environ., 663, 329-337, https://doi.org/10.1016/j.scitotenv.2019.01.262, 2019.

Zhan, Y. Z. H., Xie, M., Gao, D., Wang, T. J., Zhang, M., and An, F. X.: Characterization and source analysis of water-soluble inorganic ionic species in $PM_{2.5}$ during a wintertime particle pollution episode in Nanjing, China, Atmos. Res., 262, https://doi.org/10.1016/j.atmosres.2021.105769, 2021.

Zhang, L. L., Wilson, J. P., MacDonald, B., Zhang, W. H., and Yu, T.: The changing $PM_{2.5}$ dynamics of global megacities based on long-term remotely sensed observations, Environ. Int., 142, https://doi.org/10.1016/j.envint.2020.105862, 2020.

Zhang, Z. Z., Wang, W. X., Cheng, M. M., Liu, S. J., Xu, J., He, Y. J., and Meng, F.: The contribution of residential coal combustion to $PM_{2.5}$ pollution over China's Beijing-Tianjin-Hebei region in winter, Atmos. Environ., 159, 147-161, https://doi.org/10.1016/j.atmosenv.2017.03.054, 2017.

Zheng, H., Kong, S. F., Yan, Q., Wu, F. Q., Cheng, Y., Zheng, S. R., Wu, J., Yang, G. W., Zheng, M. M., Tang, L. L., Yin, Y., Chen, K., Zhao, T. L., Liu, D. T., Li, S. L., Qi, S. H., Zhao, D. L., Zhang, T., Ruan, J. J., and Huang, M. Z.: The impacts of pollution control measures on $PM_{2.5}$ reduction: Insights of chemical composition, source variation and health risk, Atmos. Environ., 197, 103-117, https://doi.org/10.1016/j.atmosenv.2018.10.023, 2019.

Zhou, C. S., Chen, J., and Wang, S. J.: Examining the effects of socioeconomic development on fine particulate matter ($PM_{2.5}$) in China's cities using spatial regression and the geographical detector technique: Sci. Total Environ., 619, 436-445, https://doi.org/10.1016/j.scitotenv.2017.11.124, 2018.

Zhu, Y. J., Xie, J. G., Huang, F. M., and Cao, L. Q.: Association between short-term exposure to air pollution and COVID-19 infection: Evidence from China, Sci. Total Environ., 727, https://doi.org/10.1016/j.scitotenv.2020.138704, 2020.

Zong, Z., Wang, X. P., Tian, C. G., Chen, Y. J., Qu, L., Ji, L., Zhi, G. R., Li, J., and Zhang, G.: Source apportionment of $PM_{2.5}$ at a regional background site in North China using PMF linked with radiocarbon analysis: insight into the contribution of biomass burning, Atmos. Chem. Phys., 16, 11249-11265, https://doi.org/10.5194/acp-16-11249-2016, 2016.

Zou, B. B., Huang, X. F., Zhang, B., Dai, J., Zeng, L. W., Feng, N., and He, L. Y.: Source apportionment of $PM_{2.5}$ pollution in an industrial city in southern China, Atmos. Pollut. Res., 8, 1193-1202, https://doi.org/10.1016/j.apr.2017.05.001, 2017.